COMMUNICATIONS CHEMISTRY

ARTICLE

https://doi.org/10.1038/s42004-019-0198-0 OPEN

# Probing molecular mechanisms of M13 bacteriophage adhesion

Chanoong Lim [1,3], Jina Ko [1,3], Dasom Jeon[2], Yoojung Song [1], Jinwoo Park [1], Jungki Ryu [2] & Dong Woog Lee [1]

M13 bacteriophages can provide a versatile platform for nanobiotechnology because of their unique biological and physicochemical properties. Polypeptides on their surfaces can be finely tuned on demand through genetic engineering, enabling tailored assembly of multiple functional components through specific interactions. Their versatility has been demonstrated by synthesizing various unprecedented hybrid materials for energy storage, biosensing, and catalysis. Here we select a specific type of genetically engineered M13 bacteriophage (DSPH) to investigate the origin of interactions. The interaction forces between the phage-coated surface and five different functionalized self-assembled monolayers are directly measured using a surface forces apparatus. We confirm that the phages have strong adhesion energies in acidic environments due to π-π stacking and hydrophobic interactions, while hydrogen bonding interactions remain relatively weak. These results provide quantitative and qualitative information of the molecular interaction mechanisms of DSPH phages, which can be utilized as a database of the bacteriophage interactions.

[1] Department of Chemical Engineering, School of Energy and Chemical Engineering, Ulsan National Institute of Science and Technology (UNIST), 50 UNIST-gil, Ulsan 44919, Republic of Korea. [2] Department of Energy Engineering, School of Energy and Chemical Engineering, Ulsan National Institute of Science and Technology (UNIST), 50 UNIST-gil, Ulsan 44919, Republic of Korea. [3] These authors contributed equally: Chanoong Lim, Jina Ko. Correspondence and requests for materials should be addressed to J.R. (email: jryu@unist.ac.kr) or to D.W.L. (email: dongwoog.lee@unist.ac.kr)

The discovery and identification of biomolecular interactions have improved our understanding of the unique functions of biological systems and significantly contributed to the development of nanobiotechnology. Due to the polyfunctionality of biomolecules[1], they often employ unique combinations of individual interactions (e.g., hydrogen bonding, steric hydration, electric double layer, van der Waals, cation–π, and hydrophobic interactions) and, as a result, can form strong ensemble interactions with specific molecules or matter (so called specific interaction or molecular recognition)[2–4]. These specific biomolecular interactions have been successfully employed to develop target-specific drug delivery, bioimaging, and biosensing systems[5–8]. Furthermore, various unprecedented functional materials have been developed using these interactions[9–12]. The M13 bacteriophage (or virus) is a representative example of a toolkit for such applications[13–18]. Due to its inherent nanostructure, abundant polypeptides present on its surface, and modification flexibility through genetic engineering, the M13 bacteriophage has been successfully utilized to assemble and fabricate various functional nanomaterials. Examples include hybrid materials of carbon nanotubes (CNTs) and $TiO_2$ for photovoltaics[15], CNTs and inorganic materials for rechargeable batteries[19], and porphyrin and $IrO_x$ for solar water splitting[20].

However, the polyfunctionality of biomolecules also poses a significant challenge for experimentally exploring the fundamental origins of these interactions. The unidentified origins of biomolecular interactions lead to difficulties in rationally designing new biomolecules with desired binding affinities for unexplored target molecules/matter. In the case of M13 bacteriophages, randomly mutated bacteriophage libraries were repeatedly exposed to target materials to screen specific biomolecular interactions (phage display)[21–24]. There have also been several attempts to rationally design biomolecules with molecular recognition capabilities rather than relying on serendipitous findings (e.g., phage display)[9]. However, most conventional studies have relied on empirical design rules because of the lack of proper experimental analysis and our understanding on these biomolecular interactions.

In this work, we first report the precise measurement of various interaction forces between the M13 bacteriophage and common functional groups using a surface forces apparatus (SFA) to understand the origin of its molecular recognition capability. In particular, we measure the interaction forces of the M13 virus with CNT-binding polypeptides (DSPH) along its filamentous capsid—an amino acid sequence of **DSPH**TELP on pVIII coat proteins—with various functional groups. Among various types of phages, we choose the DSPH phage for the following reasons: (1) it has a specific binding affinity toward CNTs, which can find diverse applications in various fields, such as catalysis[13], biomedical engineering[16], materials science[15], and energy conversion and storage[19]. In addition, the molecular structure of CNTs are very similar to that of other carbon materials, such as fullerene, graphene, and graphite. Thus, our study can provide valuable insights to a broader range of researchers. (2) Because the CNT-binding sequences of the DSPH phage were abundantly displayed (~2700 copies) along its filamentous structure, it can provide more reliable measurement for SFA analysis than other types of phages with the CNT-binding sequences on pIII (~five copies). In addition, a high aspect ratio and flexibility of the M13 bacteriophage make it difficult to study the interaction forces for pIII proteins. (3) Practically, the DSPH phage can be more readily prepared in a large scale compared with other types of phage due to its high amplification rate in *E. coli*. Five different types of functional groups are prepared using self-assembled monolayers (SAMs) bearing different terminal groups: carboxylic (COOH), hydroxyl (OH), amine ($NH_2$), methyl ($CH_3$), and phenyl (Ph) groups. Direct and precise measurement of the force versus distance curves with the SFA under various conditions allow the identification of different types of interaction forces between the M13 bacteriophages and functional groups. These provide clues to the molecular origin of its CNT-binding ability. Our results suggest that histidine and proline moieties play critical roles in the binding of the phages to CNTs and aggregate formation in aqueous solutions, respectively. These results are further confirmed by the pH-dependent behaviors of the phage complexation with the CNTs, indicating that aggregation and precipitation of the complexes can be tuned by pH. We believe that this study can provide a versatile platform to characterize various specific biomolecular interactions and enable better understanding and utilization of biomolecules.

## Results

**Experimental setup and contact angle measurements**. For SFA analysis (Fig. 1), we prepared a monolayer of M13 bacteriophages and SAMs with various functional groups. Mica substrates, which are frequently used for SFA analysis because of their atomically flat nature, were readily coated with DSPH phages after replacing surface $K^+$ ions with $Mg^{2+}$ ions and exposing the substrate to a phage solution (see the Methods section for details). Atomic force microscopy (AFM) confirmed the monolayer deposition of filamentous DSPH phages with uniform lengths and diameters of 880 and 6.6 nm (Supplementary Fig. 1), as reported previously[14]. Their deposition density was easily controlled by varying the concentration of the DSPH solution. For the SFA analysis, the number density was controlled to be ~30 per $\mu m^2$, because this led to the highest coverage (82%) of the mica by the DSPH phages without the formation of phage multilayers and aggregates, which can hinder the precise measurement of the interaction forces. In the case of the SAMs, each of the end-functionalized alkanethiols was deposited on a molecularly smooth gold surface (Fig. 1, see the Methods section for details). We prepared SAMs with five different end-functional groups: positively chargeable $NH_2$, negatively chargeable COOH, polar OH, aliphatic and nonpolar $CH_3$, and aromatic and nonpolar Ph groups.

Prior to the measurement of the interaction forces, the wetting properties of the DSPH and SAMs were investigated as a function of the pH and/or waiting time ($t$) because of their pH-dependent physicochemical properties (Fig. 2; see the Methods section for more details). Considering the $pK_a$ values of the tested functional groups (Supplementary Table 1) and side-chain functional groups of the DSPH phage (Supplementary Table 2), as well as the isoelectric point (pI) value of the latter (~5.3)[15], contact angles were measured at pH 3.0 and 8.5, respectively. Figure 2 shows the contact angles of the SAM-coated and DSPH-coated surfaces at these pHs. There was not a significant difference between the contact angles measured at pH 3.0 and 8.5 for most of the tested SAMs (Fig. 2a). The Ph-/$CH_3$-SAM and OH-/$NH_2$-SAM remained hydrophobic and hydrophilic, respectively, regardless of the pHs. On the contrary, the COOH–SAM showed significant differences between the contact angles at pH 3.0 ($\theta = 44.6 \pm 1.3°$) and 8.5 ($\theta = 19.9 \pm 1.4°$). Due to its $pK_a$ value of ~5.5[25], it could be deprotonated and become more hydrophilic at pH 8.5. It is noteworthy that the $NH_2$–SAM should also be pH sensitive ($pK_a$ ~7.5), but it exhibited a negligible difference in the contact angles upon pH changes[26]. The observed difference in the pH-dependent wetting properties of the COOH– and $NH_2$–SAMs can be attributed to the differences in their molecular conformations. According to the literature, the $NH_2$–SAM can form hydrogen bonding (H-bonding) networks with surrounding water molecules, regardless of its protonation state[27,28]. However, the

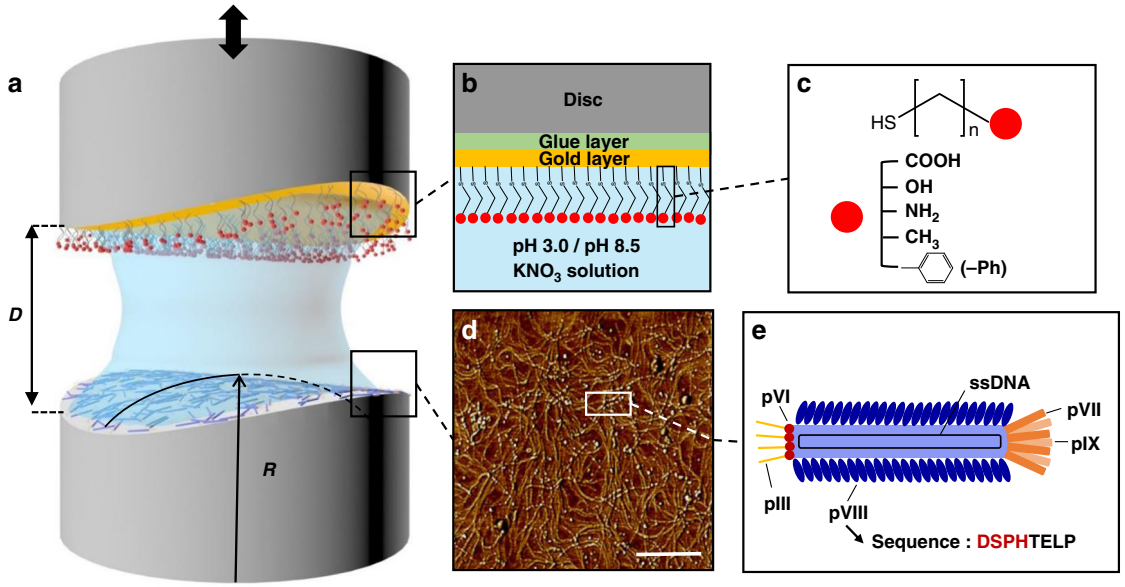


**Fig. 1** Experimental scheme. **a** Surface forces apparatus setup for measuring interaction forces between the functionalized SAM layer (top surface) and M13 bacteriophage deposited on mica (bottom surface). **b** Funtionalized SAM layer on gold surface. **c** Molecular structure of five different alkanethiols for the formation of the functionalized SAM layers. **d** AFM image of the M13 bacteriophage on mica. Scale bar, 1 μm. **e** Structure of the M13 bacteriophage

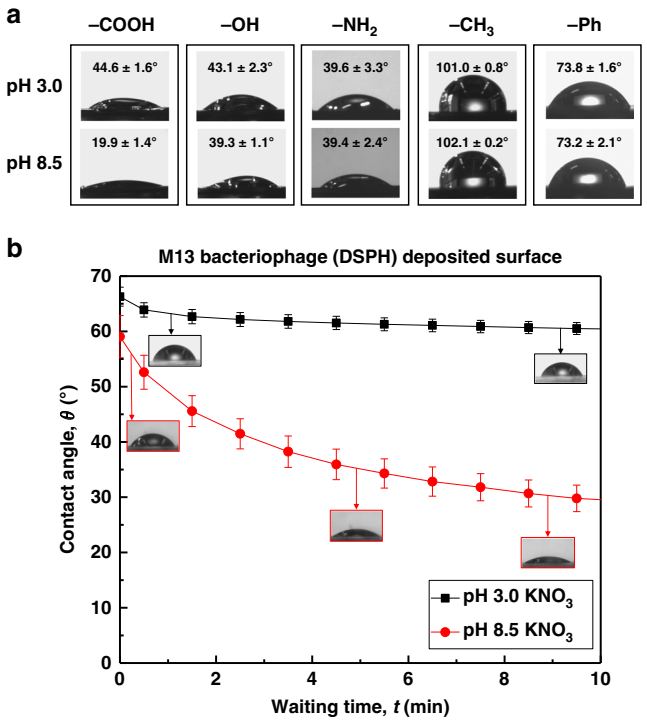


**Fig. 2** The wetting properties of the functionalized SAMs and DSPH. Contact angle values of (**a**) functionalized SAMs and (**b**) DSPH-coated surface as a function of pH and/or waiting time. The error bars represent the s.e.m. (standard error of mean), where $n \geq 7$

COOH–SAM can form intermolecular H-bonding between end-functional groups only when they are protonated, leading to the decrease in the hydrophilicity with the pH[29,30].

The wettability of the DSPH-coated surface was measured as a function of the pH and waiting time ($t$) after contact with the solution to determine the rearrangement/reorientation of the coat proteins of the bacteriophage on the mica surface (Fig. 2b). The contact angle at pH 8.5 gradually decreased from $\theta = 59.1 \pm 3.8°$ ($t = 0$ s) to $\theta = 27.1 \pm 0.6°$ ($t = 10$ min). The contact angle at pH 3.0 was relatively insensitive to the waiting time, showing a slight decrease from $\theta = 66.3 \pm 1.7°$ ($t = 0$ s) to $\theta = 60.4 \pm 1.1°$ ($t = 10$ min). Considering its pI value (~5.3), the positively charged DSPH phages at pH 3.0 could interact more strongly with the negatively charged mica surface than with water molecules, resulting in a slightly high contact angle and a negligible change over time. However, when exposed to pH 8.5, significant amounts of negatively charged amino acids (e.g., aspartic and glutamic acids) in the DSPH could reorient and become exposed to the DSPH–water interface, increasing the hydrophilicity with time. Moreover, swelling of the DSPH (which was confirmed by SFA, as presented in a later section) could increase the rotational degrees of freedom, which may have accelerated the rearrangement process[31,32].

**Interaction force measurements**. In addition to evaluating the hydrophobicity/hydrophilicity of DSPH phage and the five different functional terminated SAMs, we measured the interaction forces between the phage and the five different SAMs using SFA (Figs. 3, 4). Force versus distance profiles were measured upon approach and detachment of the DSPH- and SAM-modified surfaces to determine the adhesion force and energy ($W_{ad}$) under various conditions: pHs of 3.0 and 8.5 and contact times ($t_c$) of 5 s and 1 h.

We first measured the interaction forces at pH 3.0. The adhesion energy between the COOH–SAM and DSPH increased from $W_{ad} = 0.23 \pm 0.02$ mJ m$^{-2}$ at $t_c = 5$ s to $W_{ad} = 2.32 \pm 0.40$ mJ m$^{-2}$ at $t_c = 1$ h (Fig. 3a). The OH–SAM increased from $W_{ad} = 3.08 \pm 0.75$ mJ m$^{-2}$ at $t_c = 5$ s to $W_{ad} = 5.32 \pm 0.26$ mJ m$^{-2}$ at $t_c = 1$ h (Fig. 3b). The similar contact angles of the COOH– ($\theta = 44.6 \pm 1.6°$) and OH–SAMs ($\theta = 43.1 \pm 2.3°$) at pH 3.0 suggest that they should have similar magnitudes of hydration repulsion or hydrophobic attraction. Interestingly, despite the expected similarity in the origin of adhesion for both SAMs (i.e., H-bonding), the measured adhesion energy of the COOH–SAM was ~30–50% smaller than that of the OH–SAM. This quantitative discrepancy is attributed to the differences in the molecular conformation of their terminal functional groups in aqueous solutions. As explained earlier, the protonated

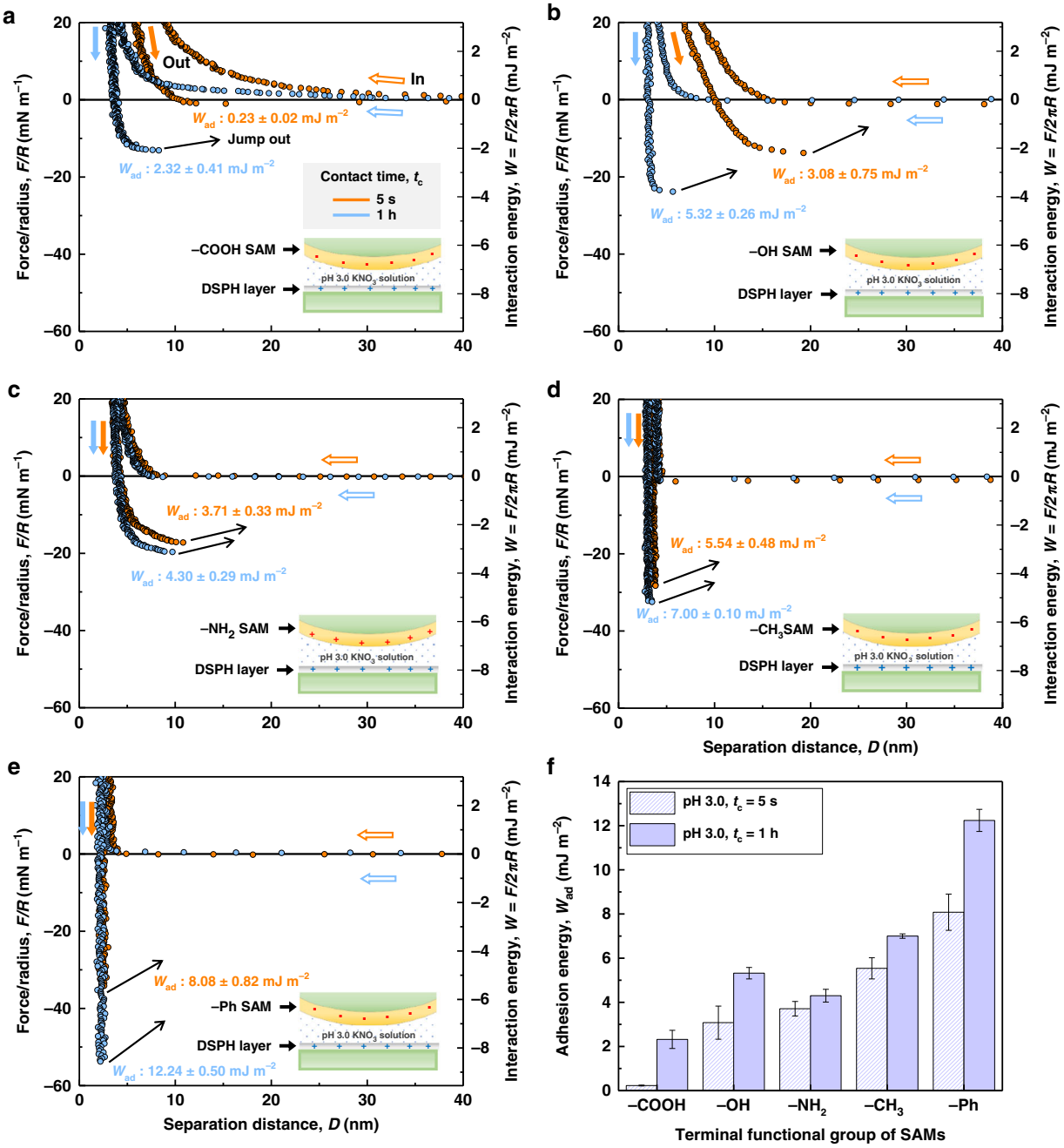


**Fig. 3** Force versus distance profiles measured at pH 3.0. The interactions force of the DSPH-coated surface was measured against SAMs with five different terminal functional groups: **a** –COOH, **b** –OH, **c** –$NH_2$, **d** –$CH_3$, and **e** –Ph. The empty and solid arrows correspond to the approach and detachment of the two surfaces, respectively. The orange and sky-blue curves correspond to the force-profiles at contact times ($t_c$) of 5 s and 1 h, respectively. **f** Bar graph showing the overall adhesion energy ($W_{ad}$) of different SAMs at pH 3.0 as a function of contact time. The error bars represent the s.e.m., where $n$ = 5 in each group

carboxylic head group (–COOH) at pH 3.0 can partially form a H-bonding with a neighboring group (–H with –O–) or a dimer (–H with = O)[29]. This suggests that the DSPH bacteriophages may have fewer chances to form H-bonding with the protonated COOH–SAM than with the OH–SAM at pH 3.0, which also coincides with a molecular dynamics simulation study by Yang et al.[33].

To our surprise, despite the positive charges of the $NH_2$–SAM and the DPSH bacteriophage at pH 3.0, the adhesion energy between them ($W_{ad} = 4.30 \pm 0.29$ mJ m$^{-2}$ at $t_c = 1$ h) was comparable with that between the OH–SAM and the bacteriophage (Fig. 3c). It was expected that H-bonding would occur between the $NH_2$–SAM and DSPH, as both are rich in H-bonding donors and acceptors. In addition to H-bonding, it was expected that additional interactions would be present because the measured force versus distance profile indicated that electrostatic repulsion between them was negligible compared with the adhesion forces. It is well known that protonated primary amines can have cation–π interactions as a cationic donor with aromatic moieties, such as histidine of the pVIII protein. Assuming that half of the pVIII proteins from the deposited phages participated in these interactions, the adhesion force per pVIII protein would be ~15.3 kcal mol$^{-1}$ (~26 $kT$). This suggests that there could be multiple cation–π interactions per pVIII protein because the

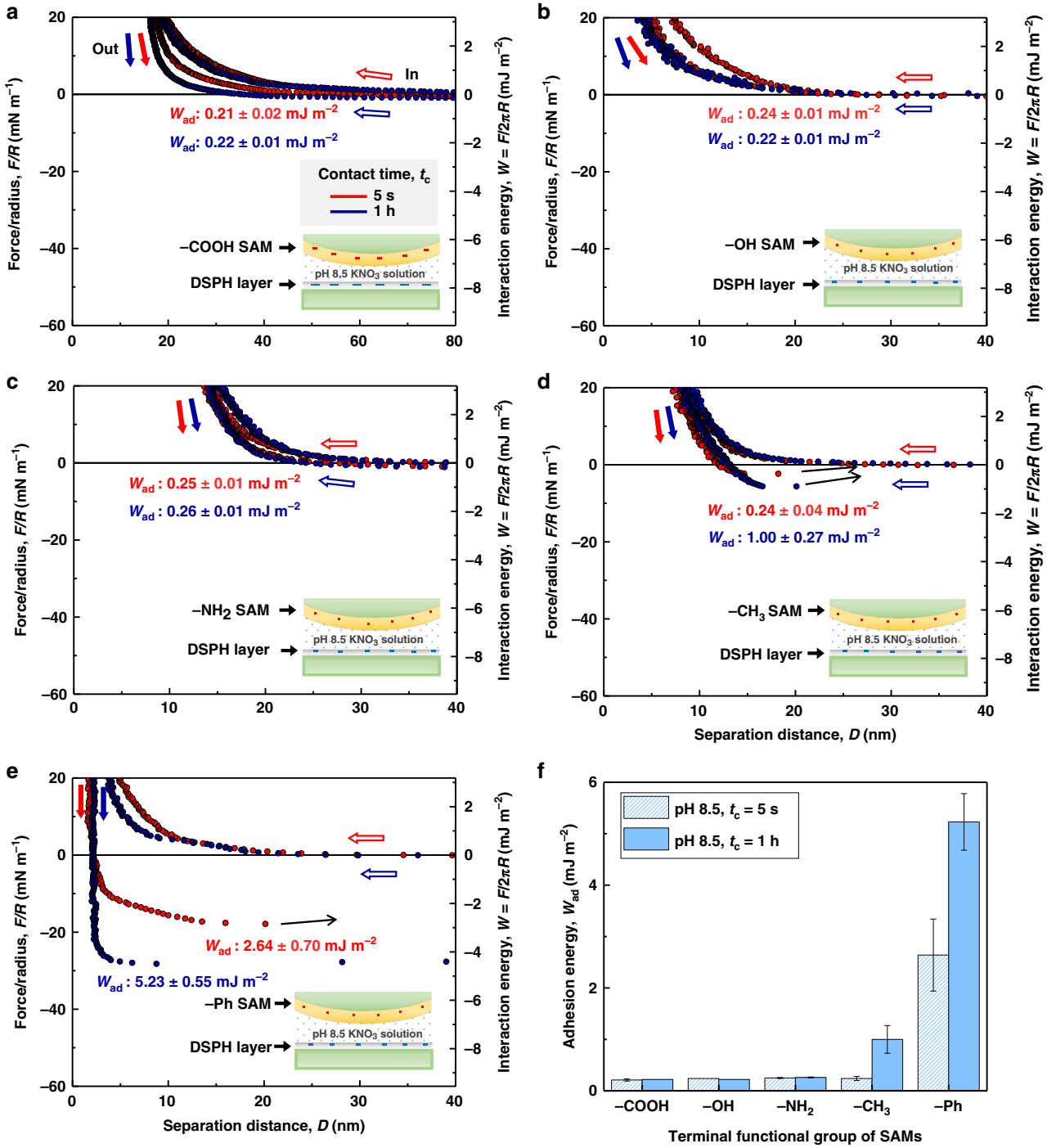


**Fig. 4** Force versus distance profiles measured at pH 8.5. The interactions force of the DSPH-coated surface was measured against SAMs with five different terminal functional groups: **a** –COOH, **b** –OH, **c** –$NH_2$, **d** –$CH_3$, and **e** –Ph. The empty and solid arrows correspond to the approach and detachment of the two surfaces, respectively. The red and blue curves correspond to the force profiles at contact times ($t_c$) of 5 s and 1 h, respectively. **f** Bar graph showing the overall adhesion energy ($W_{ad}$) of different SAMs at pH 8.5 as a function of contact time. The error bars represent the s.e.m., where $n = 5$ in each group

strength of the cation–π interaction was estimated to be ~5.5 kcal mol$^{-1}$ in water[34].

The adhesion energy between the $CH_3$–SAM and DSPH layer was significantly higher ($W_{ad} = 7.00 \pm 0.10$ mJ m$^{-2}$) compared with those of the COOH–, OH–, and $NH_2$–SAMs (Fig. 3d). The origin of the strong attraction between the DSPH and $CH_3$–SAM was most likely due to the strong hydrophobic interactions, as evidenced by the contact angle measurement, in which the $CH_3$–SAM was very hydrophobic ($\theta = 101.0 \pm 0.8°$). The approach curve indicates that any types of repulsive forces were completely overwhelmed by the strong adhesion until the surfaces became closer than their steric wall distance, $D_{sw}$ (Fig. 3d)[35]. A simple DSPH adsorption experiment on the $CH_3$– and COOH–SAM perfectly corresponded with the SFA result, which showed the deposition of a significantly denser DSPH layer on the $CH_3$–SAM compared with the COOH–SAM (Supplementary Fig. 2).

Among all the tested SAMs, the Ph–SAM exhibited the highest adhesion energy against the DSPH bacteriophage at pH 3.0

($W_{ad} = 8.08 \pm 0.82$ mJ m$^{-2}$ at $t_c = 5$ s and $W_{ad} = 12.24. \pm 0.50$ mJ m$^{-2}$ at $t_c = 1$ h) (Fig. 3e). If the strong adhesion between the phage and Ph–SAM was solely caused by hydrophobic interactions, the adhesion energy between them should be lower compared with that between the phage and $CH_3$–SAM, as the $CH_3$–SAM was more hydrophobic, as shown in Fig. 2. The strong interactions between the DSPH phage and Ph–SAM can be attributed to the π–π stacking (as hypothesized from other work), cation–π, and hydrophobic interactions. The high proportions of histidine (**H**) and proline (**P**) in the surface-exposed portion of the pVIII protein (DS**PH**TEL**P**) for the DSPH phage (~12.5 and ~25%, respectively) were closely correlated to these results. It was reported that even though proline is not a π-conjugated system at pH 3.0, it can favorably interact with the π–electron-rich phenyl aromatic face and induce the aforementioned interactions, minimizing the steric penalty[36].

Previous studies showed that the magnitude of the π–π stacking energy mediated by protonated histidine is stronger than that of deprotonated histidine[37]. In biological systems, the positively charged histidine has been known to be an important cationic source in cation–π interactions for regulating protein folding and reactivity[38]. Considering that histidine is always protonated under acidic conditions (pH 3.0), cation–π interactions would be one of the major contributors to the interactions with the Ph–SAM. Furthermore, all the amino acids' α protons could interact with the Ph–SAM via CH/π interactions, regardless of the pH conditions[36].

All the adhesion energies measured at pH 3.0 were higher at $t_c = 1$ h compared with those at $t_c = 5$ s. The increase in adhesion with $t_c$ is a typical sign of structural rearrangements or reorientation of biological macromolecules[39,40], indicating that the adhesive bonds (physical interactions, including van der Waals, H-bonding, and hydrophobic attraction in this study) developed favorably while the functional groups and DSPH were in contact. The decrease in $D_{sw}$ during contact also suggests that molecular rearrangement occurred (Supplementary Fig. 3).

In general, the adhesion energies at pH 8.5 were much lower than those in acidic conditions, regardless of the opposing functional group (Fig. 4). The increase in the hydrophilicity of the DSPH-coated surface (as shown in the contact angle measurements) and the larger $D_{sw}$ between the two opposing layers indicate the existence of strong steric- and hydration–repulsion caused by the swelling of the bacteriophages on the mica surface.

Consequently, for the COOH–, OH–, and $NH_2$–SAMs, repulsive forces dominated over all the other adhesive forces, yielding purely repulsive force versus distance profile. On the contrary, for the $CH_3$– and Ph–SAM, the adhesive forces were still stronger than the repulsive counterparts, even though significant decreases in the adhesion energies were observed at pH 8.5. The adhesion energies between the Ph–SAM and DSPH layer (~$2.64 \pm 0.70$ mJ m$^{-2}$ at $t_c = 5$ s and ~$5.23 \pm 0.55$ mJ m$^{-2}$ at $t_c = 1$ h) were still the strongest (Fig. 4e), indicating the dominance of π–π interactions due to the histidine and CH/π interactions induced by proline in the DSPH phage[36]. The plateau before the "jump-out" upon the detachment of the Ph–SAM (Fig. 4e) at pH 8.5, which was absent at pH 3.0, may indicate that highly hydrated residues of the DSPH phage were "peeled-off" before detachment (Supplementary Fig. 4).

The adhesion energy per virus can be calculated based on the number density of DSPH (calculated from AFM images) and the measured $W_{ad}$. Compared with the known dimension of DSPH (diameter ~6.5 nm)[16], adsorbed DSPH in AFM image (Fig. 1) seems to be in a "compressed cylinder" shape (lateral thickness ~20 nm) rather than a normal cylinder. Thus, 50% is a reasonable upper bound of the pVIII protein fraction directly involved in adhesion. In particular, the adhesion energy per DSPH phage on the Ph–SAM was ~$4.2 \times 10^{-16}$ J (at pH 3.0 and $t_c = 1$ h), which corresponds to ~$10^5\,kT$ at room temperature. Considering the number of pVIII proteins per M13 phage (~2700)[41], with the assumption that about 50% of the pVIII proteins were involved in the adhesion, the adhesion energy per pVIII protein was ~$74\,kT$. It is noteworthy that this value is significantly higher than the adhesion energy of well-known mussel foot proteins; the adhesion energy between a 25-mer-long mussel foot protein-3s and the hydrophobic surface was estimated to be ~$34.7\,kT$ by replica-exchange molecular dynamics (REMD) simulations[42]. Using the same assumption, the adhesion energy of one pVIII against the Ph–SAM was calculated to be ~$32\,kT$ at pH 8.5.

**Complexation and dispersion of SWCNT using DSPH phage.** Based on the finding that DSPH phage strongly interacts via π–π interaction, we investigated the pH-dependent properties of single-walled carbon nanotubes (SWCNT) and DSPH-phage complexes. The DSPH bacteriophage was reported to strongly bind with SWCNTs and maintain a stable dispersion without re-bundling[15,16], enabling diverse applications including in vitro and in vivo bioimaging and synthesis of CNT-based hybrid materials in aqueous solutions. However, little is known about the underlying mechanism for their complexation and dispersion stability, especially at high CNT concentrations. The complexation was conducted through the dialysis of a surfactant-assisted SWCNT dispersion in the presence of DSPH bacteriophages at three different pHs (pH 3.0, 5.0, and 8.5). Possible interactions between the DSPH bacteriophages and SWCNTs are listed in Fig. 5a as a function of pH. It was anticipated that π–π stacking and hydrophobic interactions were always present, regardless of the pH values. At a low pH, cation–π and electrostatic interactions may be additionally present. Due to the presence of only attractive interactions at pH 3.0 and 5.0, the dialysis of the complexing solution resulted in the formation of hazy aggregates (Fig. 5b). This seems to be contrary to previous studies that found the formation of stable SWCNT–DSPH complexes under similar conditions[15,16]. Note that we have used a much higher concentration of DSPH and SWCNTs for their complexation than previous studies; their high concentrations can decrease the separation distance and help overcome (repulsive) kinetic barriers to achieve thermodynamic equilibrium, allowing the facile acquisition of the (aggregated) global minimum state. However, we could not observe the formation of any aggregates for the sample prepared at pH 8.5. The resulting SWCNT–DSPH complex solution remained stable over 6 months without any noticeable precipitation or change. The observed high-dispersion stability of the SWCNT–DSPH complexes was attributed to the presence of additional electrostatic repulsive interactions between the complexes. The repulsive interactions can rise from negatively charged amino acids on the DSPH phage (e.g., glutamic acid and aspartic acid) and dominate over other short-range attractive interactions (e.g., π–π stacking and hydrophobic interactions). The complex mixtures were analyzed by AFM to observe the morphology of the SWCNT–DSPH complex in detail (Fig. 5c). AFM imaging and cross-section analyses showed severe aggregation of the DSPH phages and SWCNTs at pH 3.0. These results suggest that π–π stacking and hydrophobic interactions were the main driving forces for the binding of the DSPH phages with the SWCNTs, which correlated well with the SFA results. At higher pHs, the phages became negatively charged due to the deprotonation of glutamic acids and aspartic acids in the pVIII protein, increasing the electrostatic repulsion between the phages and phage-bound SWCNTs. Hence, the degree of repulsion was a major factor that affected the dispersion stabilities of the SWCNT–DSPH phage complexes. Therefore, the aggregate

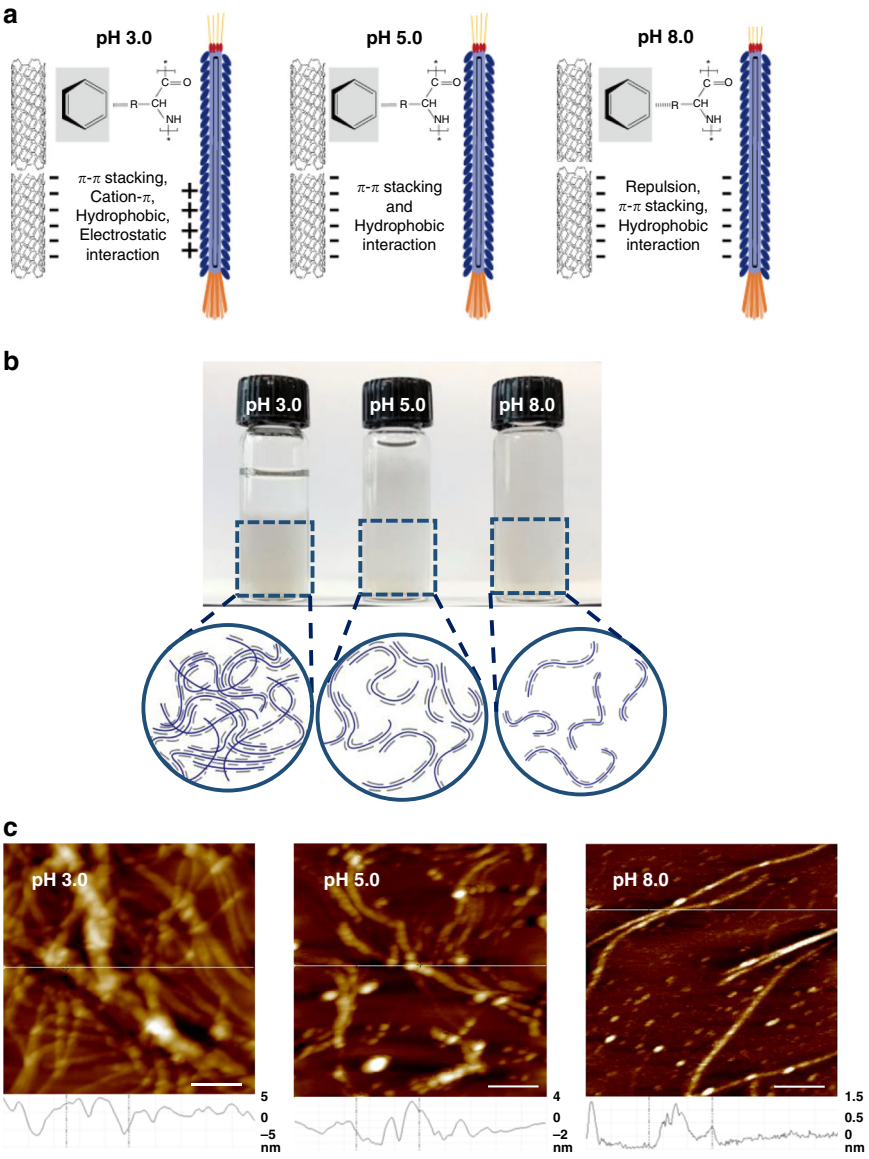


**Fig. 5** Dispersion stability of SWCNT–DSPH complex at different pHs. **a** Graphical illustration showing a list of potential interactions between the DSPH phages and SWCNTs upon their complexation. **b** Photographs of SWCNT–DSPH phage complexes prepared at different pHs: 3.0, 5.0, and 8.5. Schematic illustration explaining the observed difference in their dispersion stabilities. **c** The corresponding AFM images of SWCNT–DSPH phage complexes. Scale bar, 100 nm

formation and dispersion of SWCNTs can be simply tuned by the pH conditions when using DSPH phages as a dispersant.

## Discussion

Despite the highly consistent and reliable results, there remain a few issues that should be addressed in the future studies. First, we cannot completely exclude the possibility that another portion of the bacteriophage (e.g., pIII or pVII) other than the exposed pVIII sequences (i.e., DSPHTELP in this study) participated in the interactions with the SAMs. Second, it would be useful to measure the interaction forces of various point-mutated bacteriophages (e.g., DS**A**HTEL**A**) for a more straightforward and systematic investigation of the origin of the molecular recognition capabilities. More ideally, one can utilize the solid-phase-synthesized short peptides rather than the whole phage. Nevertheless, we believe that this study can provide insights and solid foundations for studies on specific interactions of biomolecules.

Using a model biomolecule (i.e., pVIII peptides on M13 bacteriophage with a specific sequence of DSPHTELP) and SAMs with various terminal functional groups, we could identify possible interaction forces and their strengths precisely. We found that histidine and proline moieties may play a critical role in the molecular recognition of CNTs by the DSPH phages through their engagement in attractive π interactions, as expected previously[15], and additionally through hydrophobic interactions. The measured strength of each identified interaction was comparable with previously reported values. It is thought that a much higher abundance of pVIII at the phage surface compared with other proteins allowed the SFA analysis with adequate reliability. We also experimentally demonstrated that DSPH–SWCNT complexes can be stabilized at a high pH through electrostatic and hydration repulsion.

The interaction origin of M13 bacteriophages (DSPH phages) was investigated by directly measuring interaction forces against functionalized SAMs (–COOH, –OH, $–NH_2$, $–CH_3$, and –Ph).

The overall results indicated that the DSPH phage exhibited the highest and lowest adhesion energy with the phenyl and carboxylic acid groups, respectively, indicating that the phages strongly interacted via π–π stacking and hydrophobic interactions, while the H-bonding interactions remained relatively weak. Moreover, we confirmed that DSPH phages interacted strongly with the SWCNTs in acidic conditions via the aforementioned physical interactions. Hence, pH-responsive tuning of the M13 bacteriophage–SWCNT complexes is possible. The obtained results can be used as a fundamental database in bacteriophage-based applications to enhance the performance of future phage-based templates. Furthermore, the utilized measurement protocol, using functional SAMs as opposing surfaces, can be applied to study the molecular interaction mechanisms of various bio and synthetic materials.

## Methods

**Materials**. HiPCo SWCNTs were purchased from Unidym. Unless stated otherwise, all chemicals, including 10-carboxy-1-decanethiol (95%), 11-amino-1-undecanethiol, hydrochloride (99%), 11-hydroxy-1-undecanethiol (97%), 1-undecanethiol (98%), and 2-phenylethanethiol (98%), were purchased from Sigma-Aldrich.

**Preparation of SAMs with different end-functional groups**. Each alkanethiol was prepared on atomically smooth gold surfaces. The smooth gold surfaces (thickness: 45 nm) were prepared on cleaved clean muscovite mica (Grade #1, S&J Trading. Floral Park, NY, USA) through electron beam evaporation. The gold layers were attached to the curved surfaces of cylindrical glass discs (Radius, $R$ ~2 cm) by painting them with an optical adhesive, Norland optical adhesive 81 (Norland Products, Inc. Cranbury, NJ, USA), and subsequently UV treating the samples for 40–60 min. The discs with gold-coated top surfaces were immersed into 1 mM alkanethiol-ethanol solution for the formation of SAM structure via gold-sulfur bonds on the gold (111) surfaces[43]. After 16–18 h, the discs were sonicated for 30 s, washed with ethanol, and dried by nitrogen gas to remove physical impurities and excess SAM molecules from the surfaces.

**M13 bacteriophage cultivation**. The DSPH phage was obtained from Prof. Belcher's group at Massachusetts Institute of Technology. Cultivation of M13 bacteriophages was performed using *Escherichia coli* strain ER2738 from New England Biolab. First, 10 mL of the Luria Bertani (LB) medium was mixed with 10 μL of TET (antibiotic) and a single colony of ER2738 cells, and incubated overnight. For large-scale amplification, 1 mL of TET, 10 mL of the overnight culture, and ~$10^{11}$ pfu of the DSPH phage were added to a freshly prepared LB medium (25 g of LB medium and 1 g of $MgCl_2.6H_2O$ in 1 L of distilled water). Thus, around $10^{14}$ pfu $mL^{-1}$ of bacteriophages were produced. Finally, the culture was incubated at 37 °C in a shaker for 225–250 rpm for about 6 h.

**Bacteriophage purification**. First, 500 mL of the culture was poured into each large centrifuge tube and centrifuged at 7800 rpm for 30 min. After centrifugation, 70 mL of PEG/NaCl (200 g of PEG and 146 g of NaCl in 1 L deionized water) was added to a 420 mL of supernatant, and the mixture was left overnight at 4 °C. The solution was centrifuged again at 8140 rpm for 30 min, the supernatant was discarded, and the solution was centrifuged at 8140 rpm for another 5 min. The white phage pellets in the centrifuged solution were dissolved completely in a 30 mL of TBS solution. The solution was centrifuged at 10,000 rpm for 5 min to remove residual impurities, after which 5 mL of PEG/NaCl solution was added to the solution and mixed until the solution became homogeneous. Finally, the phage solution was centrifuged at 11,000 rpm for 30 min, the supernatant was discarded, and the solution was centrifuged again at 11,000 rpm for 5 min. The resulting phage solution concentration was determined by the amount of the white phage pellets that were obtained just before centrifuging to dissolve the 1 mL TBS solution (pH 7.2).

**Preparation of monolayer M13 bacteriophage surface**. An atomically smooth mica surface was treated with a 0.1 M $MgCl_2$ solution to replace $K^+$ ions with $Mg^{2+}$ ions on the surface of the mica before the deposition of the phages[44]. The mica substrate was subsequently treated with an M13 solution (pH 5.0) to deposit a monolayer of M13 bacteriophages through electrostatic attractions between the positively charged mica and negatively charged M13 phages. An appropriate concentration of the M13 bacteriophage solution for the preparation of a monolayer M13 phage film for SFA analysis was $2.74 \times 10^{12}$ pfu $mL^{-1}$ (Supplementary Fig. 1), according to morphology investigations with a Veeco multimode V_AFM in standard tapping mode. A drop (80 μL) of the M13 bacteriophage solution was loaded on the $MgCl_2$-treated mica surface and left for 1 h. Finally, the surface was rinsed with deionized water and dried with nitrogen gas. The number density and coverage of the M13 bacteriophages on the mica substrate were analyzed using the freeware, ImageJ.

**Contact angle measurements**. Wetting properties of the M13 bacteriophages and alkanethiol compounds were investigated using a DSA-100B-basic contact angle analyzer (KRÜSS GmbH, Germany). First, 4 μL of 3 mM $KNO_3$ solution (pH 3.0 and pH 8.5) was dropped on each SAM surface. The contact angle values were obtained in tangent 1 fitting mode. In the case of the M13 bacteriophage-coated surface, a sample was placed in an acryl box with wetted tissues and left for 10 min to achieve air saturation, after which a 4 μL droplet of 3 mM $KNO_3$ (pH 3.0 and pH 8.5) was placed on the phage surface. The measurements were recorded as a video clip for 10 min to investigate the contact angle profile over time. Every measurement was repeated at least four times.

**Measurement of interaction forces using an SFA**. Molecular interactions and the absolute separation distances between two surfaces were measured in an asymmetric system with the Surface Forces Apparatus 2000 (Surforce LLC, Santa Barbara, CA, USA). A freshly cleaved back-silvered mica and gold surface were glued onto each cylindrical glass disc (Radius $R$, ~2 cm) using an optical adhesive, Norland optical adhesive 81 (Norland Products, Inc. Cranbury, NJ, USA). The SAMs deposited on the gold layers were placed onto the upper discs. The DSPH phage layer on the back-slivered mica was placed on the lower disc. The two opposing surfaces were arranged with a cross-cylindrical geometry in the SFA chamber, and 50 μL of a 3 mM $KNO_3$ solution (pH 3.0 and 8.5) was injected between the surfaces. The SFA chamber was thoroughly sealed and maintained for 30 min after the injection of each solution to achieve equilibration. The contact time ($t_c$) effects were also investigated by taking measurements first at $t_c = 5$ s and followed by at $t_c = 1$ h. All measurements were conducted at room temperature ($T = 23$ °C).

Force versus distance profiles were measured at a constant rate of 5 nm $s^{-1}$. The normal force $F$ was calculated as a function of the absolute surface separation distances $D$ as follows: $\Delta F(D) = k\ (\Delta D_{\text{applied}} - \Delta D_{\text{means}})$, where $k$ is the double-cantilever spring constant of 1225.8 N $m^{-1}$. The distances $D$ were confirmed from fringes of equal chromatic order (FECO) by using multiple-bean interferometry (MBI) in real time. The forces were normalized by their radii ($R$ ~2 cm) as $F_{\text{curved}}(D)\ R$ for the cylindrical discs. The normalized force $F/R$ was converted to the interaction energy per unit area $W$ between the two flat surfaces based on the Derjaguin approximation, $W_{\text{flat}}(D) = F_{\text{curved}}(D)/2\pi\sqrt{R_1 R_2} = F_{\text{curved}}(D)/2\pi R$, with $R_1 = R_2$. The adhesion energy was obtained using the Johnson–Kendall–Roberts (JKR) model, which is useful for soft materials with large deformations, $W_{\text{ad}} = 2F_{\text{ad}}/3\pi R$[39]. Each experiment was repeated, at least three times at the same contact point to investigate hysteresis effect, and at least at three different contact points under the same conditions for reproducibility and repeatability.

**SWCNT–DSPH phage complexation**. Before complexation with the DSPH phages, SWCNT (HiPCo™, diameter: 0.8−1.2 nm, length: 100−1000 nm) dispersions were prepared using a 2 wt% sodium cholate surfactant based on a previous report[15]. The DSPH phage and SWCNTs were mixed at a molar ratio of 5:1 (SWCNTs:DSPH phage) with a final concentration of DSPH phages of $1.0 \times 10^{12}$ pfu $mL^{-1}$. The SWCNT–DSPH solution mixture was first dialyzed against water (10 mM NaCl) at pHs of 3.0, 5.0, and 8.5 for complexation. Dialysis was conducted overnight with frequent solution changes.

## Data availability

The authors declare that all data supporting the findings of this study are available within the article and its supplementary information files. Additional data related to this study can be requested from the corresponding author upon reasonable request.

Received: 29 April 2019 Accepted: 29 July 2019
Published online: 20 August 2019

## References

1. Beveridge, D. L. et al. Liquid state computer simulations of biomolecular solvation problems. *Ann. N. Y. Acad. Sci.* **367**, 108–131 (1981).
2. Johnson, E. R. et al. Revealing noncovalent interactions. *J. Am. Chem. Soc.* **132**, 6498–6506 (2010).
3. Dougherty, D. A. Cation-π interactions in chemistry and biology: a new view of benzene, Phe, Tyr, and Trp. *Science* **271**, 163–168 (1996).
4. Cosic, I. Macromolecular bioactivity: is it resonant interaction between macromolecules?-theory and applications. *IEEE Trans. Biomed. Eng.* **41**, 1101–1114 (1994).
5. Park, J. et al. Polydopamine-based simple and versatile surface modification of polymeric nano drug carriers. *ACS Nano* **8**, 3347–3356 (2014).
6. Meng, H.-M. et al. Aptamer-integrated DNA nanostructures for biosensing, bioimaging and cancer therapy. *Chem. Soc. Rev.* **45**, 2583–2602 (2016).

7. Shin, Y. C. et al. Cell-adhesive RGD peptide-displaying M13 bacteriophage/PLGA nanofiber matrices for growth of fibroblasts. *Biomater. Res.* **18**, 14–20 (2014).
8. Ghosh, D. et al. M13-templated magnetic nanoparticles for targeted in vivo imaging of prostate cancer. *Nat. Nanotechnol.* **7**, 677–682 (2012).
9. Grigoryan, G. et al. Computational design of virus-like protein assemblies on carbon nanotube surfaces. *Science* **332**, 1071–1076 (2011).
10. Lee, H.-E. et al. Amino-acid-and peptide-directed synthesis of chiral plasmonic gold nanoparticles. *Nature* **556**, 360–365 (2018).
11. Dorval Courchesne, N. M.-M., Steiner III, S. A., Cantú, V. J., Hammond, P. T. & Belcher, A. M. Biotemplated silica and silicon materials as building blocks for micro-to nanostructures. *Chem. Mater.* **27**, 5361–5370 (2015).
12. Guterman, T. et al. Electrical conductivity, selective adhesion, and biocompatibility in bacteria-inspired peptide–metal self-supporting nanocomposites. *Adv. Mater.* **31**, 1807285 (2019).
13. Lee, S. Y., Lim, J. S. & Harris, M. T. Synthesis and application of virus-based hybrid nanomaterials. *Biotechnol. Bioeng.* **109**, 16–30 (2012).
14. Kim, W.-G. et al. Biomimetic self-templating optical structures fabricated by genetically engineered M13 bacteriophage. *Biosens. Bioelectron.* **85**, 853–859 (2016).
15. Dang, X. et al. Virus-templated self-assembled single-walled carbon nanotubes for highly efficient electron collection in photovoltaic devices. *Nat. Nanotechnol.* **6**, 377–384 (2011).
16. Yi, H. et al. M13 phage-functionalized single-walled carbon nanotubes as nanoprobes for second near-infrared window fluorescence imaging of targeted tumors. *Nano Lett.* **12**, 1176–1183 (2012).
17. Chung, W.-J., Merzlyak, A. & Lee, S.-W. Fabrication of engineered M13 bacteriophages into liquid crystalline films and fibers for directional growth and encapsulation of fibroblasts. *Soft Matter* **6**, 4454–4459 (2010).
18. Lee, J. H. et al. Production of tunable nanomaterials using hierarchically assembled bacteriophages. *Nat. Protoc.* **12**, 1999–2013 (2017).
19. Lee, Y. J. et al. Fabricating genetically engineered high-power lithium-ion batteries using multiple virus genes. *Science* **324**, 1051–1055 (2009).
20. Nam, Y. S. et al. Biologically templated photocatalytic nanostructures for sustained light-driven water oxidation. *Nat. Nanotechnol.* **5**, 340 (2010).
21. Mao, C., Liu, A. & Cao, B. Virus-based chemical and biological sensing. *Angew. Chem. Int. Ed.* **48**, 6790–6810 (2009).
22. Yoo, S. Y., Chung, W.-J., Kim, T. H., Le, M. & Lee, S.-W. Facile patterning of genetically engineered M13 bacteriophage for directional growth of human fibroblast cells. *Soft Matter* **7**, 363–368 (2011).
23. Yoo, S. Y., Shrestha, K. R., Jeong, S.-N., Kang, J.-I. & Lee, S.-W. Engineered phage nanofibers induce angiogenesis. *Nanoscale* **9**, 17109–17117 (2017).
24. Moon, J.-S. et al. M13 bacteriophage-based self-assembly structures and their functional capabilities. *MINI-Rev. Org. Chem.* **12**, 271–281 (2015).
25. Vezenov, D. V., Noy, A., Rozsnyai, L. F. & Lieber, C. M. Force titrations and ionization state sensitive imaging of functional groups in aqueous solutions by chemical force microscopy. *J. Am. Chem. Soc.* **119**, 2006–2015 (1997).
26. Zhang, H., He, H.-X., Wang, J., Mu, T. & Liu, Z.-F. Force titration of amino group-terminated self-assembled monolayers using chemical force microscopy. *Appl. Phys. A* **66**, S269–S271 (1998).
27. Liu, D., Wyttenbach, T. & Bowers, M. T. Hydration of protonated primary amines: effects of intermolecular and intramolecular hydrogen bonds. *Int. J. Mass spectrom.* **236**, 81–90 (2004).
28. Liu, D., Wyttenbach, T., Barran, P. E. & Bowers, M. T. Sequential hydration of small protonated peptides. *J. Am. Chem. Soc.* **125**, 8458–8464 (2003).
29. Winter, N., Vieceli, J. & Benjamin, I. Hydrogen-bond structure and dynamics at the interface between water and carboxylic acid-functionalized self-assembled monolayers. *J. Phys. Chem. B* **112**, 227–231 (2008).
30. Zhao, J., Luo, L., Yang, X., Wang, E. & Dong, S. Determination of surface pKa of SAM using an electrochemical titration method. *Electro. (N. Y. N. Y.)* **11**, 1108–1113 (1999).
31. Rupley, J. A. & Careri, G. Protein hydration and function. *Adv. Protein Chem.* **41**, 37–172 (1991).
32. Bone, S. & Pethig, R. Dielectric studies of protein hydration and hydration-induced flexibility. *J. Mol. Biol.* **181**, 323–326 (1985).
33. Yang, A.-C. & Weng, C.-I. Influence of alkanethiol self-assembled monolayers with various tail groups on structural and dynamic properties of water films. *J. Chem. Phys.* **129**, 154710 (2008).
34. Hu, J., Barbour, L. J. & Gokel, G. W. The indole side chain of tryptophan as a versatile π-donor. *J. Am. Chem. Soc.* **124**, 10940–10941 (2002).
35. Israelachvili, J. N. *Intermolecular and Surface Forces* (Academic press, London, 2011).
36. Zondlo, N. J. Aromatic–proline interactions: electronically tunable CH/π interactions. *Acc. Chem. Res.* **46**, 1039–1049 (2012).
37. Liao, S.-M., Du, Q.-S., Meng, J.-Z., Pang, Z.-W. & Huang, R.-B. The multiple roles of histidine in protein interactions. *Chem. Cent. J.* **7**, 44–55 (2013).
38. Yamada, S. Cation−π interactions in organic synthesis. *Chem. Rev.* **118**, 11353–11432 (2018).
39. Lee, D. W., Lim, C., Israelachvili, J. N. & Hwang, D. S. Strong adhesion and cohesion of chitosan in aqueous solutions. *Langmuir* **29**, 14222–14229 (2013).
40. Lim, C., Lee, D. W., Israelachvili, J. N., Jho, Y. & Hwang, D. S. Contact time-and pH-dependent adhesion and cohesion of low molecular weight chitosan coated surfaces. *Carbohydr. Polym.* **117**, 887–894 (2015).
41. Flynn, C. E., Lee, S.-W., Peelle, B. R. & Belcher, A. M. Viruses as vehicles for growth, organization and assembly of materials. *Acta Mater.* **51**, 5867–5880 (2003).
42. Levine, Z. A. et al. Surface force measurements and simulations of mussel-derived peptide adhesives on wet organic surfaces. *Proc. Natl Acad. Sci. USA* **113**, 4332–4337 (2016).
43. Guo, Q. & Li, F. Self-assembled alkanethiol monolayers on gold surfaces: resolving the complex structure at the interface by STM. *Phys. Chem. Chem. Phys.* **16**, 19074–19090 (2014).
44. Adamczyk, Z., Zaucha, M. & Zembala, M. Zeta potential of mica covered by colloid particles: a streaming potential study. *Langmuir* **26**, 9368–9377 (2010).


## Acknowledgements

This work was supported by grants from the National Research Foundation of Korea funded by the Korean Government (NRF-2019R1A2C2005854 and NRF-2017M3A7B4052802).

## Author contributions

C.L. and J.K. designed and performed the surface characterization and SFA measurements. D.J. and J.P. cultivated M13 bacteriophage. Y.S. performed AFM analysis. J.R. and D.W.L. supervised this project. C.L., J.K., J.R., and D.W.L. wrote the paper. All authors read and approved the final paper.

## Additional information

**Supplementary information** accompanies this paper at https://doi.org/10.1038/s42004-019-0198-0.

**Competing interests:** The authors declare no competing interests.

**Reprints and permission** information is available online at http://npg.nature.com/reprintsandpermissions/

**Publisher's note:** Springer Nature remains neutral with regard to jurisdictional claims in published maps and institutional affiliations.